IEEE Access
Multidisciplinary | Rapid Review | Open Access Journal

Received October 25, 2020, accepted November 3, 2020, date of publication November 10, 2020, date of current version December 1, 2020.

Digital Object Identifier 10.1109/ACCESS.2020.3037105

Green Light Optimal Speed Advisory System Designed for Electric Vehicles Considering Queuing Effect and Driver's Speed Tracking Error

ZHAOLONG ZHANG[1], YUAN ZOU[1], (Senior Member, IEEE), XUDONG ZHANG[1], (Member, IEEE), AND TAO ZHANG[2], (Graduate Student Member, IEEE)

[1]School of Mechanical Engineering, Beijing Institute of Technology, Beijing 100081, China
[2]China North Vehicle Research Institute, Beijing 100072, China

Corresponding authors: Yuan Zou (zouyuanbit@163.com) and Xudong Zhang (xudong.zhang@bit.edu.cn)

This work was supported in part by the National Natural Science Foundation of China under Grant 51775039, Grant 51861135301, and Grant 51805030; and in part by the Special Program for Science and Technology Funding for Innovative Talents under Grant 3052019009.

ABSTRACT The GLOSA (Green Light Optimal Speed Advisory) system provides speed advice to drivers so that drivers can pass through congested intersections at right instant with shorter time and lower energy consumption. Traditional GLOSA system only considers the SPaT (Signal Phase and Timing) of traffic light. However, two another important factors, namely queuing effect and actual tracking error of drivers, are seldomly considered, which degrades the actual performance of the GLOSA system. Intelligent connected vehicles based on V2I (Vehicle to Infrastructure) have great application potential in solving this problem. In this study, firstly, a vehicle queue length estimation method based on V2I technology is proposed to predict the effective green light time. Secondly, a hierarchical GLOSA system is developed, where the upper layer provides the global recommended optimal speed aiming at minimizing energy consumption, while the bottom layer provides the modified recommended speed considering the driver's tracking error. Finally, the tracking error of the driver when executing the recommended speed is derived based on the real-world experiment. Corresponding simulation and field test platforms are also established. Results show that compared with the traditional GLOSA system, the improved GLOSA system considering the vehicle queuing effect and driving error can effectively improve the energy-saving performance of the vehicle.

INDEX TERMS Energy-saving, queuing effect, speed advice, tracking error.

I. INTRODUCTION

The increasing traffic activities not only greatly improve the mobility of people and goods, but also produce more greenhouse gas emissions and consume a lot of energy [1]. In the past decade, researchers have been looking for effective solutions to reducing transportation-related energy consumption. Therefore, many optimization methods for ecological driving are proposed, which can be divided into three categories: 1) Task-level optimization: focusing on finding a route with minimum energy consumption, namely route planning [2], [3]. 2) Strategy-level optimization: focusing on optimal control to make power sources' working states suitable for various road conditions and driving styles [4], [5]. 3) Operation-level optimization: focusing on guiding driver's operation style with the help of driver assistance system (DAS) to reduce driving energy consumption. However, due to the difference of different drivers' driving style, the energy-saving performance of DAS can be extremely distinct. The difference can be as high as 30% [6], [7]. Connected eco-driving technology, which integrates vehicle-to-infrastructure (V2I) and Vehicle to Vehicle (V2V) wireless communication, is expected to become one of the most promising candidate technologies to reduce urban traffic energy consumption.

The associate editor coordinating the review of this manuscript and approving it for publication was Liang-Bi Chen.

Among various eco-driving application schemes, the Green Light Optimal Speed Advisory (GLOSA) system is the easiest to be promoted and applied [8]. In GLOSA scenarios, vehicles obtain Signal Phase and Timing (SPaT), traffic signal information through V2I communication, and plan the optimal speed trajectory to the intersection so that unnecessary stop and go behavior at signalized intersections of main roads can be avoided, which can improve economic performance and save traveling time [9], [10].

Considering the upcoming traffic signal, [11] used a dynamic speed planning algorithm, and [12] used Model Predictive Control (MPC) cruise algorithm to maximize the probability of encountering a green light signal when approaching to multiple intersections, and avoid full parking to reduce fuel consumption. [13] proposed a robust and optimal ecological driving strategy to reduce the parking probability at uncertain timed traffic signal intersections. GLOSA Most existing researches on eco-driving ideally assume that vehicles are running in a smooth traffic flow environment. In fact, when passing a green light, vehicles may be interrupted or restricted by vehicles ahead or waiting in line. To incorporate the queue effect into the GLOSA system, real-time traffic flow information is necessary. For the advanced scenario where the penetration of connected vehicles is high and V2V communication is achievable, there exist a lot of researches investigating the cooperative control method for multiple vehicles to increase the enrgy-saving performance of the vehicle fleet [14], [15]. However, at the early development stage of intelligent transportation, the penetration of connected vehicles is low, V2V is not available in most cases. Thus, relying on the fixed traffic observer to obtain the traffic flow information and pass this information to the host connected vehicle through V2I information is more feasible. As for the researches about GLOSA which considers queue effect, [16] conducted simulation to investigate the influence of queuing effect on eco-driving strategy, but the optimal speed was not obtained. In addition, the deterministic kinematic model (DKM) [17], [18] and the traffic flow model [19] are also used in the simulation analysis of intersection queue prediction. Previous studies focused on the ecological driving control of traditional diesel locomotives. However, as the advancement of transportation electrification, electric vehicles will become the main participants of future transportation. Because electric vehicles have different configuration compared with traditional fuel vehicles and can recover energy from regenerative braking, thus it is important to investigate the effectiveness of the GLOSA system for electric vehicles.

The GLOSA system can only provide a reference or recommended speed, while the actual performance of GLOSA system heavily relies on driver's ability to track the recommended speed. To evaluate the real-world energy-saving performance of GLOSA system, road test is necessary. In [20], the authors developed an Eco-Approach and departure (EAD) application system for actuated signal to calculate the maximum or minimum time to an intersection. EAD can be seen as an modified version of GLOSA. In addition, the authors of [21] conducted a preliminary field test in riverside, California, to evaluate the energy-saving performance of the system. However, the above-mentioned tests are not enough to evaluate the performance of the EAD system because few external interference factors are included, which is not sufficient to reflect the real sophisticated urban traffic environment. To mitigate the above-mentioned research gap, [22] introduced the design method of EAD test scenarios in detail, and analyzed the impact of energy saving system on driver's behavior through real vehicle test. Results show that the system saved 2% energy in all trips. Despite the contribution of reference [22], it still has certain application limitations because it ignores the queuing effect in the actual traffic environment and the driver's driving error.

In the GLOSA system, few studies have considered human driver error [20], [23]. The conventional ecological driving technology assumes that the driver can follow the instructions accurately, which is not the case in reality. The numerical simulation results in reference [20] show that the fuel-saving performance of connected vehicles can reach 10% if the optimal speed is followed accurately, while in the real test of [23], the economic performance improvement of EAD system is only 2%. The difference in fuel-saving can be deduced to be at least partly caused by human driver's driving error in trying to follow the recommended speed.

In this paper, a GLOSA system for electric vehicles, which considers the queuing effect and human driving error, is designed and evaluated through simulation and road test. The main contributions of this paper are concluded as follows: firstly, based on the monitored traffic flow, the queue length of vehicles at intersections is estimated, and the effective green light time model is constructed. Secondly, the optimal control problem is constructed, and a hierarchical control framework is proposed. In particular, the upper level calculates the optimal speed trajectory through global planning to minimize energy consumption, while the bottom layer considers the actual tracking error of drivers and uses Stochastic Model Predictive Control (SMPC) to conduct a local adaptive speed planning. Finally, the effectiveness of the system is validated through simulation and road tests. The proposed framework in this paper is oriented at the scene where the number of connected vehicles is limited. The method tries to guide the driver's driving behavior so that the energy-saving potential under human-driving can be maximumly excited. GLOSA can be used to take over the system to execute adaptive cruise control mode, which depends on the driver's mode selection

II. VEHICLE DYNAMIC MODEL AND OPTIMAL CONTROL PROBLEM FORMULATION

A. VEHICLE DYNAMICS

The one-dimensional longitudinal dynamic model of the vehicle is constructed as Eq.(1), where the tire slip is ignored

and the vehicle is regarded as a rigid particle:

$$\begin{aligned}\dot{x}(t) &= f(x(t), u(t)) \\ &= \begin{bmatrix} 0 & 1 \\ 0 & \dfrac{-gf\cos\theta}{v(t)} - \dfrac{g\sin\theta}{v(t)} - \dfrac{0.5\rho A C_d v(t)}{m} \end{bmatrix} x(t) \\ &\quad + \begin{bmatrix} 0 \\ \dfrac{1}{m} \end{bmatrix} u(t) \end{aligned} \tag{1}$$

where x is the state variable, $x = [dv]^{\mathrm{T}}$, which is the combination of driving distance d and velocity v. u is the control variable, which is the vehicle traction force F, positive for propulsion and negative for braking. θ is the road incline. ρ is the air density. C_d is the air drag coefficient. A is the frontal area. g is the gravitational acceleration. f is the rolling resistance coefficient. It should be noted that m is the vehicle's weight which has incorporated the rotational mass.

In the traction process, the driving force of the vehicle is only provided by the motor while the force in the braking process includes the motor force and friction braking force, and the electric power is used for braking energy recovery. The relationship among vehicle force, motor force and friction braking force is shown in Eq.(2).

$$F = \begin{cases} F_m & if\ F > 0 \\ F_m + F_{bf} & if\ F \le 0 \end{cases} \tag{2}$$

where F_m is the motor force, positive for propulsion and negative for braking. F_{bf} is the friction braking force. In the braking process, the ideal regenerative braking strategy proposed by [24] is adopted

The vehicle is powered by the battery to drive the motor and auxiliary equipment. The power conversion relationships are as follows:

$$P_m = F_m r_w \frac{n\pi}{30} \tag{3}$$

$$P_b = [P_m \eta_m^{-\mathrm{sign}(P_m)} \eta_b^{-\mathrm{sign}(P_m)}] + P_a \eta_{\mathrm{b}}^{-1} \tag{4}$$

where P_m represents the motor power, P_b represents the battery power, P_a is the sum of auxiliary power. n is the wheel rotational speed. r_w is the wheel radius. η_m is the motor efficiency. η_b is the battery efficiency. sign( ) is the signum function. When P_m is greater than or equal to 0, sign(P_m) is 1. When P_m is negative, sign(P_m) is -1.

B. OPTIMAL CONTROL PROBLEM FORMULATION

As shown in Fig.1 (a), the red dotted line in Zone A is the optimal energy-saving speed derived from the residual time of traffic signal $[t_0, t_{red}]$ without considering the influence of queuing effect. Here, t_0 is defined as the starting time when the main vehicle entering the road section, t_{red} is the end time of the red light signal.

However, due to the vehicle queue at the intersection, the optimal speed is often not feasible in actual traffic scenarios. In this context, when planning the recommended speed, the GLOSA system must consider the influence of vehicle

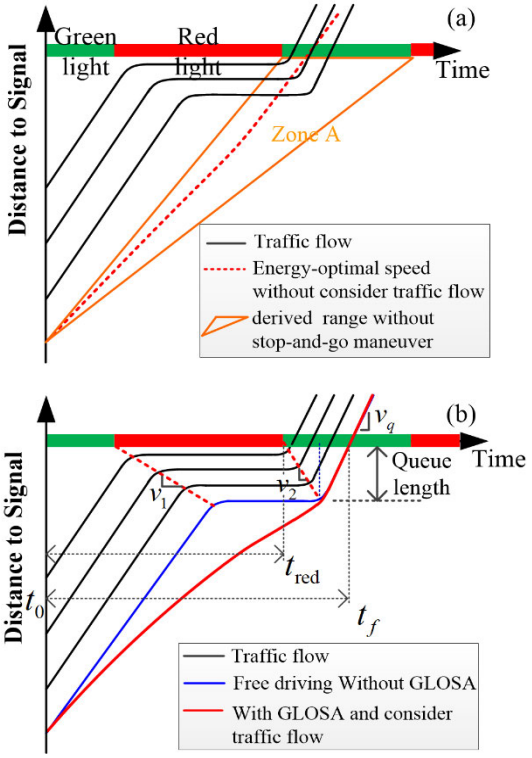

FIGURE 1. The GLOSA system at the signalized intersection. (a) Without considering queuing effect. (b) Considering queuing effect.

parking queue at the intersection. An ideal optimal speed trajectory considering queuing effect is shown in Fig.1 (b), where the guidance system ensures that the vehicle can track the end vehicle without stopping and pass the signalized intersection safely and efficiently.

To realize the proposed GLOSA system, vehicles need to have V2I communication equipment. In addition, a flow observer is needed to monitor the traffic flow of fixed-point section in the upstream of a signalized intersection. According to the traffic flow information and SPaT, the effective green light starting time t_f for the main vehicle to ensure non-stop can be calculated. $d(t)$ is the travel distance function of the host vehicle. At start time t_0, the host vehicle's location is defined as the initialization of the system, namely $d(t_0) = 0$. The host vehicle's location to the intersection is D. J is the energy consumption during the investigated time window. The optimization target is to minimize the total energy consumption of the vehicle when passing through the signalized intersection, as shown in Eq.(5):

$$\min_{u(t)} J(u(t), x(t)) = \int_{t_0}^{t_f} P_b\, dt \tag{5}$$

$$\begin{aligned} &\text{s.t}\ \dot{x}(t) = f(x(t), u(t)), \\ &\quad d(t_0) = 0, d(t_f) = D, \\ &\quad d(t_f) < v_q \end{aligned} \tag{6}$$

where $x(t) = [d(t), v(t), p(t)]$ denotes the state vector of traveled distance, speed, and energy consumption. $u(t)$ is the

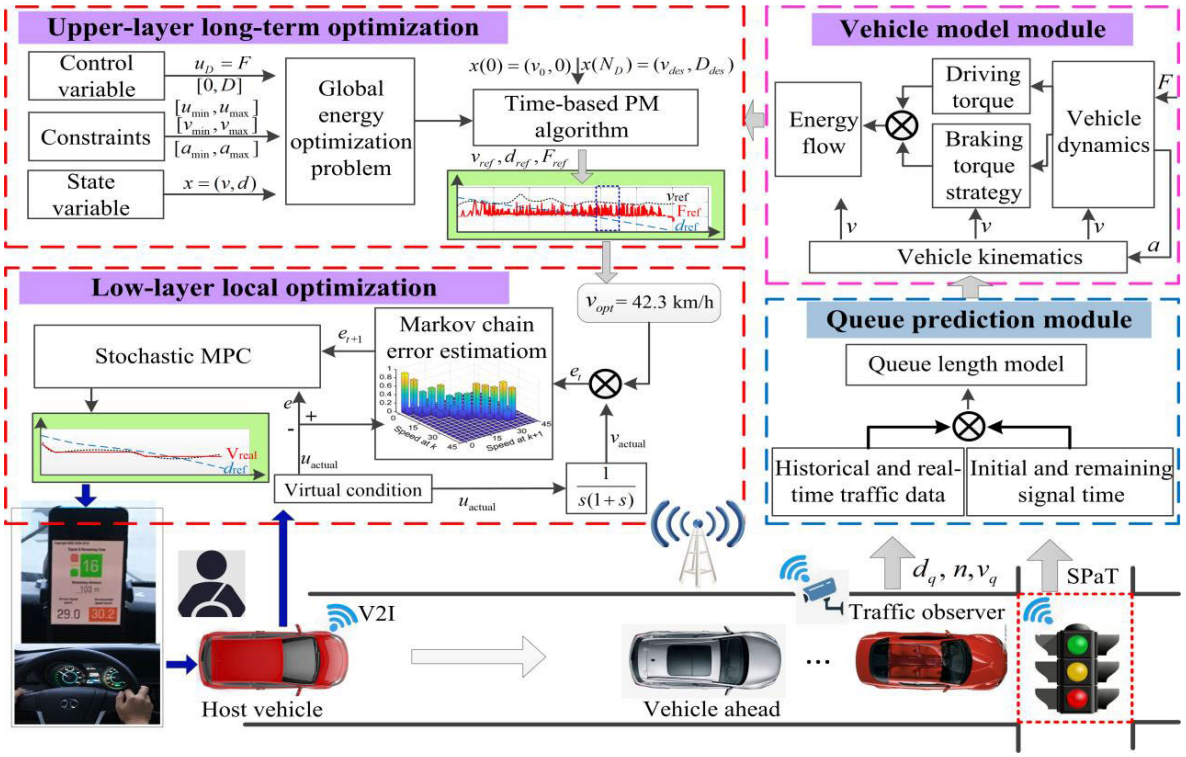

FIGURE 2. The hierarchical control framework of the proposed GLOSA system.

control input. The constraint $d(t_f) < v_q$ is required because the speed of the host vehicle when it reaches the intersection should be smaller than the average speed of the traffic flow so as to avoid collision.

The lower and upper bounds for state and control variables are as follows:

$$\begin{aligned} u_{\min} &\le u(t) \le u_{\max}, \\ v_{\text{low}} &\le v(t) \le v_{\text{limt}}, \\ a_{\min} &\le a(t) \le a_{\max}, \\ \dot{a}(t) &\le \dot{a}_{\max} \end{aligned} \tag{7}$$

where $\dot{a}_{\max}$ is the maximum allowed jerk, which is used to depress the change of vehicle acceleration thus improving driving comfort. $a_{\min}$ and $a_{\max}$ are minimum and maximum acceleration limits respectively. In addition to the maximum speed limit v_{limit}, the minimum speed limit v_{low} also needs to be defined, because driving too slowly might lead to traffic jams. Finally, the control force needs to satisfy physical limits u_{min} and u_{max}, which are the maximum braking and propulsive force, respectively. Simultaneously, constraints like the motor's maximum speed, maximum torque and speed-torque property are also considered when designing the control strategy.

C. CONTROL FRAMEWORK

A complete GLOSA system consists of queue prediction module, vehicle model module, optimization module, and onboard display module. An appropriate arrangement of these modules' working logistics is crucial. In this paper, a hierarchical framework is proposed to solve the global optimal control problem. In the upper layer, the pseudo-spectral method (PM) is used to obtain the optimal speed trajectory. Considering the drawback that the driver's tracking error is not incorporated in the upper layer, in the bottom layer, an online SMPC method is proposed to follow the optimal speed trajectory from the upper layer in a finer time step. The complete control framework is shown in Fig.2.

In the queue prediction module, by combing the historical and current traffic flow information, together with SPaT, the real-time estimation of queue length at the intersection can be obtained. The vehicle model module is used to construct the vehicle dynamic model and calculate the required driving power. Based on the estimated queue length, SPaT, state of the host vehicle, the upper-layer long-term optimization module establishes the global optimal control problem and gives out corresponding global optimal advisory speed. Finally, the low-layer local optimization module gives out the modified optimal advisory speed incorporating consideration of driver's tracking error based on SMPC algorithm. SPaT can be delivered either via cellular communication from centralised server or V2I communication from signals. However, limited to the function of our test vehicle, which only support V2I communication rather than cellular communication, the control framework relies V2I communication to obtain SPaT information.

III. QUEUE LENGTH ESTIMATION METHOD

The research object of this paper is the main electric vehicle with V2I function, and the fixed detector is installed in the upstream of the intersection to monitor the cross-section traffic flow and regional speed. Both the detector and the traffic signal system have communication ability.

When estimating the vehicle queue length at the intersection, the actual traffic congestion state needs to be identified. When the traffic flow at intersection is smooth, based on shock wave theory [25], the maximum queue length encountered by the main vehicle at the intersection is:

$$L_{\max} = \frac{v_1 v_2 R}{v_2 - v_1} \tag{8}$$

where v_1 is the speed of the converging wave generated by the traffic flow when the red light starts. v_2 is the dissipated wave speed generated by the dissipated vehicle when the green light is on. In the unsaturated flow v_2 is always larger than v_1. R represents the starting time of green light. The schematic diagram of queuing shock wave is shown in Fig.3.

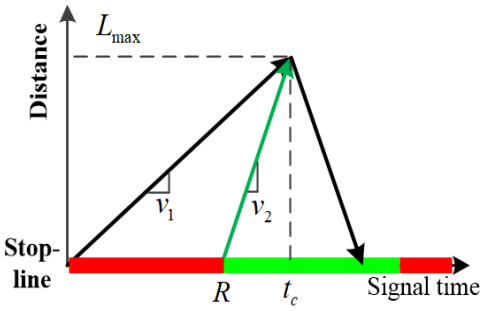

FIGURE 3. The schematic diagram of queuing shock wave.

In the i th interval, assuming that the 5-min detection flow of the ith time interval is N_i, then the arrival rate $q(i) = 12N_i$ *veh/h*. Let $k(i)_j$ denote the density of vehicle queue and $k(i)_a$ denote the density of arriving vehicles in the ith time interval, then according to the shock wave theory, the velocity of the accumulation wave at the ith time interval is

$$v(i)_1 = \frac{12N_i}{k(i)_j - k(i)_a} \tag{9}$$

where $k(i)_a$ can be calculated by road traffic speed $v(i)$ and traffic flow $q(i)$:

$$k(i)_a = \frac{q(i)}{3.6v(i)} = \frac{N_i}{0.3v(i)} \tag{10}$$

The dissipated wave velocity of the ith interval can be calculated according to the traffic capacity and the traffic density at the time of dissipation. Assuming that the traffic capacity of the intersection obtained by statistics is CAP, the dissipated wave velocity is:

$$v(i)_2 = \frac{CAP}{k(i)_m - k(i)_j} \tag{11}$$

where $k(i)_m$ represents the dissipation vehicle density at ith time interval and can be calculated according to the traffic capacity and vehicle speed:

$$k(i)_m = \frac{CAP}{3.6v(i)} \tag{12}$$

Therefore, the estimated queue length of the ith interval $(L_2)_i$ is:

$$(L_2)_i = \frac{\frac{\lambda N_i}{k(i)_j - k(i)_a} \frac{CAP}{k(i)_m - k(i)_j}}{\frac{CAP}{k(i)_m - k(i)_j} - \frac{\lambda N_i}{k(i)_j - k(i)_a}} \tag{13}$$

where λ is the number of detection times within 1 hour. Eq.(8)$\sim$ Eq.(13) are used to demonstrate the method for queue length estimation. When the method is finally applied in reality, the time interval and λ needs to be carefully chosen according to the traffic situation of the investigated intersection. According to the queue length L_2, dissipated wave velocity $v(i)_2$ and vehicle arrival speed v_q, the impassable time in Fig.1(b) can be derived as:

$$t_f = t_{red} + L_2/v_2 + L_2/v_q \tag{14}$$

So the effective traffic light model can be expressed as:

$$s(t) = \begin{cases} 0, & t \in [t_0,\ t_f] \\ 1, & t \in (t_f, t_{green}] \end{cases} \tag{15}$$

where $s(t)$ is the status of the ith traffic light: 1 represents the light is green and 0 represents the light is red; t_{green} represents the time when the green light ends. In this paper, the proposed estimation method uses the real-time traffic information from the traffic observers as the input. Even if there are network vehicles ahead, its influence on the queue length still can be captured by the traffic observer because the obtained traffic flow information is a holistic result of all traffic participants whether the vehicle is connected or not. Therefore, the proposed method is still useful and relatively accurate under the scenario where there are multiple network vehicles ahead.

IV. HIERARCHICAL CONTROL POLICY

A. UPPER LAYER OPTIMIZATION

The upper optimization layer is used to provide the optimal speed with minimum energy consumption. The driving distance and speed are taken as the state variables and the traction force of the vehicle is selected as the control variable. In order to ensure that the vehicle arrives at the intersection within t_f and the traffic speed meets the safety requirements, it is necessary to provide additional terminal speed and distance constraints. Here, additional penalty will be added to the objective function if the terminal condition is not met:

$$\min_{u(t)} J(u(t), x(t)) = \int_{t_0}^{t_f} P_b\, dt + \gamma_1 (v(t_f) - v_{end})^2 + \gamma_2 (d(t_f) - D)^2 \tag{16}$$

where γ_1, γ_2 are the weight coefficients for speed error and distance error respectively. The proposed optimal control

problem can be solved numerically by the gradient-based method provided by the pseudo-spectral optimal control software. As a typical direct method for solving nonlinear programming (NLP) problems, PM has been fully verified in terms of its optimality and applicability, and has been widely used to solve the optimal control problems of various dynamic systems [26], [27].

The PM algorithm uses orthogonal matching points to discretize the continuous optimal control problem, and approximates the state and control variables by global interpolation polynomials, thus transforming the problem into an NLP problem. This method has the advantages of high precision, low sensitivity to an initial value, and fast convergence speed, and is convenient to deal with terminal constraint problems. In [28], [29], the calculation process of the PM algorithm has been introduced in detail, and has been successfully applied to the energy management of hybrid electric vehicles. The PM algorithm can obtain the same global optimal solution as dynamic programming (DP) in a shorter time. For the sake of simplicity, this paper does not repeat the calculation process of the PM algorithm for simplicity.

B. LOWER LAYER OPTIMIZATION

Under the condition of manual driving, the GLOSA system can broadcast the optimal recommended speed to the driver according to the optimal solution given by the upper layer. However, the driver cannot track the optimal speed accurately. Therefore, the goal of the lower layer is predicting the driver's tracking error and providing appropriate speed suggestions for the main vehicle, so that the actual driving speed is as close as possible to the calculated optimal vehicle trajectory. The algorithm used in the lower layer is SMPC [30], [31], whose current control action is obtained by solving a finite time-domain open-loop optimal control problem at each sampling moment while considering the stochastic interference factors. The control framework of the lower layer is shown in Fig.2.

The driving error $\omega(t)$ is defined as the difference between acceleration calculated by the recommended speed trajectory and driver's real acceleration. According to the observation along the time axis, the human error in the next time step usually depends on the current error, and the error characteristics of different drivers are different. Thus, inspired by this Markovian property [32], [33], Markov chain, which is represented by the probability transition matrix, is used to model human driving error to reflect the random behavior of drivers.

According to the probability transition matrix learned from historical driving data, the future driving error can be estimated according to current observed tracking error. In order to obtain the driving error of acceleration, firstly, the actual driving data v_{real} of the driver tracking the reference speed v_{ref} should be collected from the road test, and the corresponding acceleration a_{real} and a_{ref} can be calculated. Then the difference between a_{real} and a_{ref} is calculated for every second and the error is discretized into finite intervals, whose number is N_e. Finally, the transition times of driving error between different levels are counted, and the transition probability matrix T_e can be obtained.

$$T_e = \begin{bmatrix} e_{11} & e_{21} & \cdots & e_{N_e 1} \\ e_{12} & e_{22} & \cdots & e_{N_e 2} \\ \vdots & \vdots & \ddots & \vdots \\ e_{1N_e} & e_{2N_e} & \cdots & e_{N_e N_e} \end{bmatrix} \tag{17}$$

where e_{ij} represents the probability of error state transition from state i to j, where $i, j \leq N_e$, For a specific driver, assuming his/her driving behavior is stable, thus his/her driving error transition probability matrix is fixed.

After T_e is obtained, the error change path probability tree containing different step sizes can be generated according to the current error state. Fig.4 shows an example of an error change path, where $N_e = 4$ and time step $N_s = 4$. The initial error at t_0 is known. The error at t_1 is obtained by referring T_e. Based on the error at t_1, the error at t_2, t_3, and t_4 can be obtained by cycle calculation. The number above the red arrow represents the corresponding state transition probability, and the probability of the example error change path in Fig.4 is $P = 0.56 \times 0.44 \times 0.72 \times 0.31 = 0.0022$. When all paths are combined, 4^4 probability paths can be obtained.

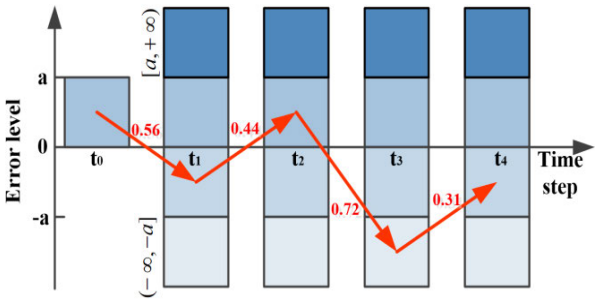

FIGURE 4. Example of error change path.

It should be noted that the increase of N_e and N_s will significantly increase the number of paths, that is, increase the computational burden. In order to realize the real-time application of the proposed algorithm, the Monte Carlo method is used to sample the paths with higher probability [34]. The specific operation is to generate a random number using uniform distribution. If the generated number is between jth and the $(j+1)$th cumulative transition probability value for current step error, then the jth error level is the next step error.

In human based closed-loop control system, human input error can be deemed as a disturbance source. The receding horizon property of SMPC allows the system to better handle predictable disturbances. The nonlinear longitudinal dynamic model of Eq.(1) also applies to the lower layer, but the control variable in the lower layer is $u_f(t)$, which is a combination of modified control variable $u_a(t)$ in the upper layer and human input error $\omega(t)$:

$$\begin{aligned} u_f(t) &= u_a(t) + \omega(t) \\ u_a(t) &= u(t)/m \end{aligned} \tag{18}$$

where $u_a(t)$ is the optimal tractive force per unit mass suggested by the upper system. $\omega(t)$ can be understood as the error injected by the human when trying to follow the advised u. Within finite time steps, different state trajectory has different human error trajectory. SMPC is used to solve the optimization problem of human error uncertainty in each finite time steps.

The vehicle dynamic model needs to be discretized when applying SMPC. To reduce the computational burden, we employ the approximate linearization method to transform the nonlinear time-varying vehicle longitudinal dynamics to a linear time-varying (LTV) system. Then, the vehicle longitudinal dynamics Eq.(1) can be rewritten as:

$$\dot{x}_{ref}(t) = f(x_{ref}(t), u_f(t)) \tag{19}$$

where, $x_{ref}(t) = [\ d_{ref}\ \ v_{ref}\ ]^{\mathrm{T}}$, d_{ref} and v_{ref} are the reference vehicle states given by the upper layer, respectively. By expanding the right side of Eq.(10) using Taylor series around the reference point and discarding the high-order terms, the following vehicle state error model can be derived:

$$\dot{\tilde{x}}(t) = \begin{bmatrix} 0 & 1 \\ 0 & -\dfrac{\rho A C_d v_{ref}(t)}{m} \end{bmatrix} \tilde{x}(t) + \begin{bmatrix} 0 \\ \dfrac{1}{m} \end{bmatrix} \tilde{u}_f(t) \tag{20}$$

Furthermore, according to the probability P_s of each possible path, the cost function of SMPC is defined as the expected square error of the reference speed v_{ref} and the predicted speed v_{pred} in the specified time steps:

$$E(v - v_{ref})^2 = \sum_{s=1}^{N_{mc}} p_s \sum_{K=t+1}^{t+l} [v_{pred}(k) - v_{ref}(k)]^2 \tag{21}$$

where N_{mc} is the number of sampling paths by the Monto Carlo method. t represents the current time, l is the optimization horizon. Here, we use 1s as the sampling period because it will not only reduce the computational burden but also avoid too frequent updates to facilitate the driver to track the recommended speed. To sum up, the optimal control problem based on SMPC can be expressed as follows:

$$\arg\min u_f \sum_{s=1}^{N_{mc}} p_s \sum_{K=t+1}^{t+l} [v_{pred}(k) - v_r(k)]^2 \tag{22}$$

V. SIMULATION AND REAL WORLD EXPERMENT

A. DRIVER TRACKING ERROR DATA ACQUISITION

Most of existing GLOSA system can only be run on the computer platform or embedded controllers. The GLOSA system that can be used for real-vehicle application is still rare to see. Therefore, we develop a simple ecological driving broadcast system, and the complete test platform is shown in Fig.5.

1) Inertial navigation system NAV982-GNSS is installed at the vehicle centroid position to obtain the vehicle speed and acceleration. The inertial navigation also provides vehicle GPS coordinate information for real-time update of vehicle travel distance.

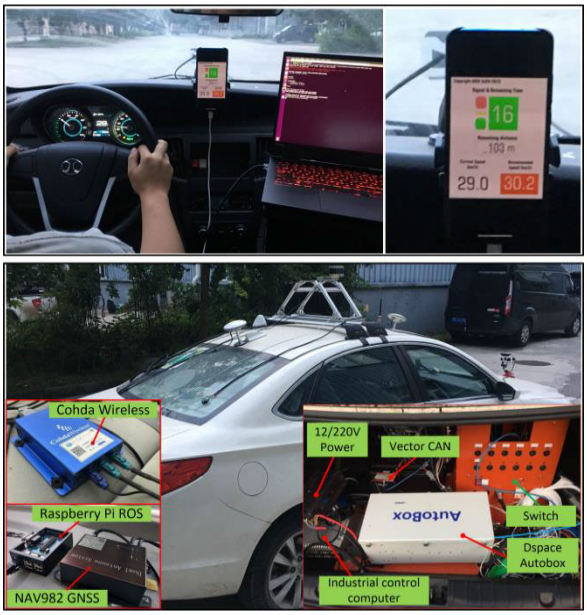

FIGURE 5. Developed GLOSA test platform.

2) Robot Operating System (ROS) is used to construct a real-time speed display system [35]. The system can display the recommended speed, remaining distance and SPaT information on the mobile phone screen.

3) Traffic flow statistics equipment is placed at the fixed point upstream of the intersection and communicates with the test vehicle by Cohda wireless in real-time. BeiQi EU vehicle is used as the field test vehicle.

In the process of data collection, we use the preset recommended speed to prompt the driver. The interface update frequency is 1Hz, and the recommended speed range is from 10km to 60km. All drivers should follow the recommended speed instead of driving freely. When the actual speed exceeds a certain range of recommended speed, the driver is warned by voice. Note that the recommended speed should be as flat as possible otherwise too frequent and sharp speed changes will cause the driver's disgust and confusion. In this study, the data acquisition and the follow-up road test adopt the same interface standard to eliminate the error introduced by the broadcast system. In the experiment, we recruited six experienced drivers and let them drive on real traffic roads to track the preset speed.

The acceleration error is divided into five positive and negative intervals, namely $(-\infty, -0.8\text{m/s}^2)$ $(-0.8\text{m/s}^2, -0.6\text{m/s}^2)$ $(-0.6\text{m/s}^2, -0.4\text{m/s}^2)$ $(-0.4\text{m/s}^2, -0.2\text{m/s}^2)$ $(-0.2\text{m/s}^2, 0)$ $(0, 0.2\text{m/s}^2)$ $(0.2\text{m/s}^2, 0.4\text{m/s}^2)$ $(0.4\text{m/s}^2, 0.6\text{m/s}^2)$ $(0.6\text{m/s}^2, 0.8\text{m/s}^2)$ $(0.8\text{m/s}^2, +\infty)$. Number 1-10 are used to represent the above ten error levels. Two typical types of speed tracking error are shown in Fig.6, where x-axis represents the error level at current time, y-axis represents the error level at next time. Because both x-axis and y-axis represent the acceleration error level, their coordinate scales are the same. For example, number 1 in both x-axis and y-axis

represents the error level $(-\infty, -0.8\text{m/s2})$. The error levels of the x-axis and y-axis are the same. In Fig.6(a), the driver's error is mainly concentrated on the diagonal line, which can be interpreted as that the driver's driving behavior is stable, so the error difference between adjacent time steps is small. The error transition probability in Fig.6(b) more appears in the extra off-diagonal direction, which means the driver is more likely to take short-term variability aggressive driving.

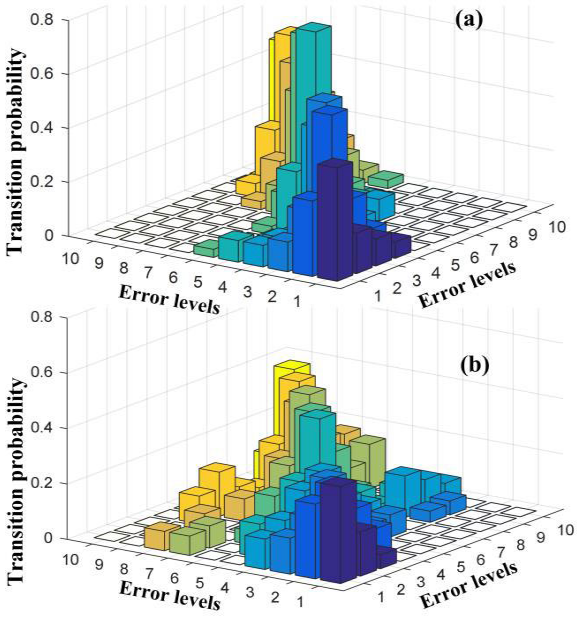

FIGURE 6. Transition probability matrix for two typical types of speed tracking error.

FIGURE 7. Test road and traffic flow observer.

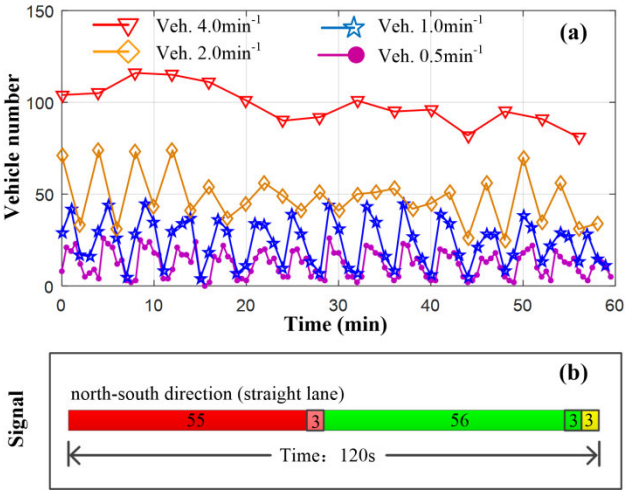

FIGURE 8. Traffic flow monitored by observer.

B. NUMERICAL SIMULATION

In this paper, the simulation only considers the traffic flow data of the target intersection, and assumes that the vehicles are evenly distributed on all lanes. Other external factors like parking, lane changing, non-motor vehicle interference, etc. are not considered. The intersection used for simulation is a main road in Beijing. The traffic flow detector is arranged at 200m upstream of the intersection. The test road and traffic flow observer are shown in Fig.7.

The monitored data at one day's morning rush hour is used for analysis. The monitored traffic flow for different time spans is shown in Fig.8(a). The SPaT of the traffic light at the intersection is shown in Fig.8(b). From Fig.8(a), it can be seen that when time span decreases to 0.5min or 1min, the traffic flow curve demonstrates periodic fluctuation, which is caused by the signal lamp truncation effect. This periodic characteristic implies that if a short time span is used, the short-term future traffic flow can be approximated and predicted by historical data.

Taking the traffic flow during 9:30 to 10:30 in the morning as an example, the parameters of Eq.(13) after calibration are $\lambda = 120$, $\text{CAP} = 1650$ *pcu/h*, $k(i)_j = 140$ *pcu/km*. The queue length is calculated every 5 minutes and compared with the historical statistical queue length. The results are shown in Fig.9. It can be seen that the queue length estimated based on the section flow data is very close to the measured real value. In addition, the estimated length can be appropriately enlarged to further ensure that the traffic has become smooth when the main vehicle arrives at the intersection. By the way, more traffic observers may help to increase the traffic flow prediction accuracy.

To verify the effectiveness of the proposed GLOSA framework, one method is to compare it with other algorithms of the same kind. However, this may be time-consuming and laborious. In order to highlight the novelty of this paper that driver's tracking error is incorporated into the GLOSA system, we compare the GLOSA with and without considering driver's tracking error to demonstrate the superiority of the proposed hierarchical framework. Table 1 lists the main parameters of the main vehicle and other traffic parameters of the investigated intersection used in simulation are listed in Table 2.

For comparison, the intelligent driver model (IDM) is used as a reference for different driving modes to simulate the

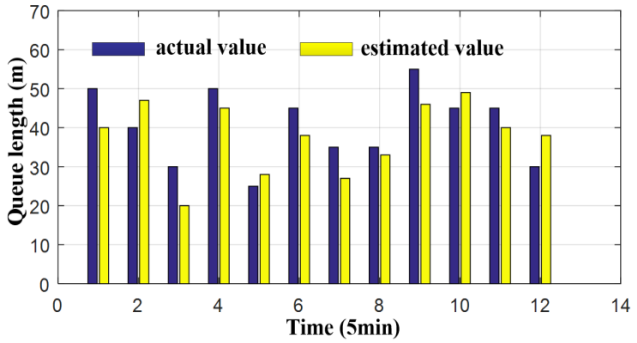

FIGURE 9. Real and estimated queue length.

TABLE 1. Vehicle paramters.

parameter	value	parameter	value
Mass m, kg	1583	Battery Efficiency	0.9
Front area A, m^2	2.21	Tire radius, m	0.325
Maximun power, kW	50/100	C_D	0.3
Maximun power, Nm	145/260	ρ, $kg.m^{-3}$	1.206
Maximum speed, km/h	140	δ	1.021
Auxiliary power, W	200	f	0.015

TABLE 2. Scenario paramters.

parametert	value	parametert	value
Distance, m	700	Initial speed, km/h	62
Minimum speed, km/h	20	Red signal time, s	58
Maximum speed, km/h	70	Green signal time, s	62
Average speed, km/h	62	Traffic flow, Veh/0.5min	12-14

dynamic of queue movement at intersections. IDM model is a widely accepted traffic flow model used for a single lane, which can be used to describe the dynamic behavior of human driving or self-driving vehicles [36]. It can be described as:

$$\begin{cases} d_{des} = \Delta s - v s_i / 2\sqrt{a^{\max} a_c} \\ \dot{v}_{\text{IDM}} = a^{\max}[1 - (v/v^{\max})^4 - (d_{des}/s_i)^2] \end{cases} \tag{23}$$

where d_{des} is the desired inter-vehicle clearance, Δs represents the safety distance, s_i is the real inter-vehicle distance, $a^{\max}$ is the maximum allowed vehicle acceleration, and a_c is the preferred deceleration considering driving comfort.

To explicit the influence of traffic flow on optimal speed planning, three control strategies are compared by simulation, namely, fixed speed driving using IDM, eco-driving without considering queuing effect and proposed GLOSA considering queuing effect, which is represented by the yellow solid line, green solid line, and red dashed line in Fig.10. The blue line indicates the parking vehicle queue. Due to the queuing effect, the effective green light starting time for the main vehicle delays to at about 56s rather than 45s when the traffic light turns to green in reality. It can be seen from Fig.10 that under the constant speed driving mode, the IDM follows the traffic flow to the intersection, and stops to wait until the queue moves again. For the traditional GLOSA system without considering the queuing effect, if the main vehicle keeps tracking the global optimal trajectory, it may lead to rear-end collision at the intersection. For the optimal trajectory considering queuing effect, the main vehicle reduces its driving speed when approaching the intersection to avoid parking behavior.

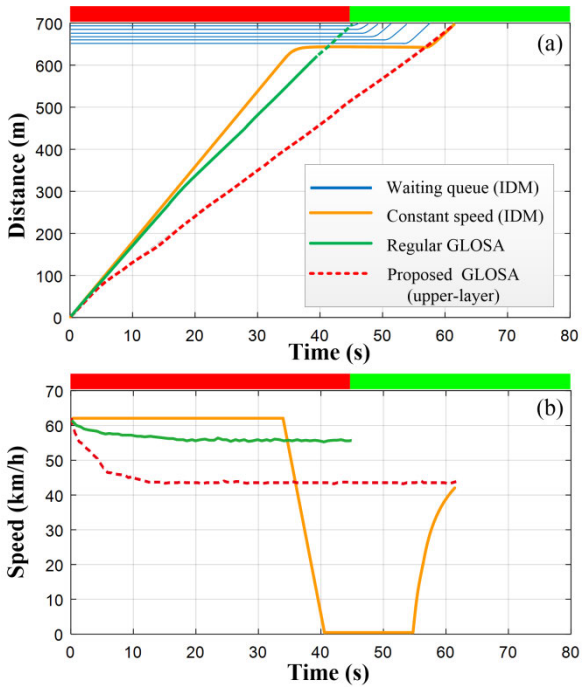

FIGURE 10. Recommended speed trajectories of three different control algorithms.

In the simulation for the lower layer, because there is no real driver in the system, the driving error probability transition matrix constructed before is used to simulate the real human driver's tracking error. In addition, it is also used as the driving error input for the SMPC model.

The simulation results are shown in Fig.11. In Fig.11(a), the driver just tracks the optimal speed trajectory given by the upper layer. It can be seen that due to the accumulation of human driving tracking error, compared with the recommended speed, the tracking error in the simulation gradually becomes larger. If the driver keeps tracking the global optimal trajectory, it may lead to rear-end collision at the intersection as the driver's tracking speed is larger than the planned speed. Fig.11(b) shows the modified recommended speed through SMPC in lower layer in purple dotted line. The blue solid line is the driver's tracking speed. Note that the benchmark recommended speed is recalculated three times (which have been labeled by red arrows) in the simulation. If the update

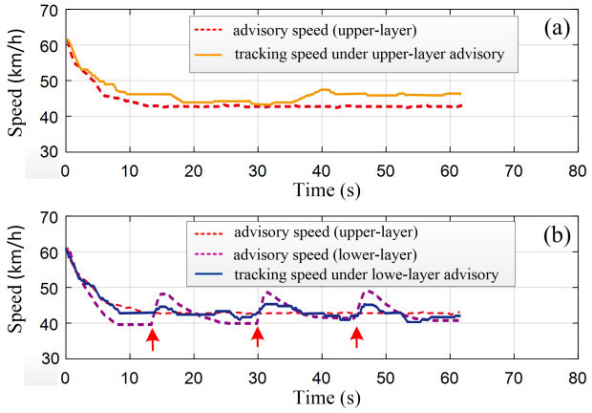

FIGURE 11. Simulation results with/without considering tracking error.

calculation of SMPC is too frequent, the modified recommended speed will change frequently, which is not conducive to the driver's tracking in the real scene. Although SMPC gives a new reference speed after considering the driver's tracking error, the final driving speed trajectory in Fig.11(b) still deviates from the recommended optimal speed due to unavoidable human errors. However, compared with the tracking error in Fig.11(a) without considering driving error, the speed trajectory in Fig.11(b) is closer to the optimal speed trajectory (red dotted line) given by the upper layer.

Due to the inevitable reaction delay and tracking error, there is always a difference existing between optimal trajectory and real trajectory. The above difference has a certain impact on energy efficiency. Based on the simulation data and Eq.(1-4), the energy consumption without considering driving error and considering driving error increase by 7.38% and 6.51%, respectively. Compared with the former, the latter realizes 11.8% improvement in energy-saving performance. This is because the tracking error is considered in the lower layer, so the driver's real speed trajectory when following the modified recommended speed trajectory is closer to the planned optimal speed.

In order to ensure the algorithm's real-time performance, the optimization process of each update cycle needs to be completed within 1s. Fig.12 shows the calculation time for different combinations of horizon length and error level in the Linux system. It can be seen that the calculation time increases rapidly when the number of error levels or horizon lengths increases. To keep a balance between computational burden and control accuracy, the number of error levels is set as 10 and the horizon length is set as 15 steps. Corresponding calculation time is 0.89s, which satisfy the 1s calculation time constraint. Therefore, the lower layer control program updates every 15s, which is consistent with the update period in Fig.11.

VI. EXPERIMENT RESULT ANALYSIS

A. EXPERIMENTAL DESIGN

To verify the effectiveness of the proposed hierarchical GLOSA system, a real-vehicle experiment was conducted on

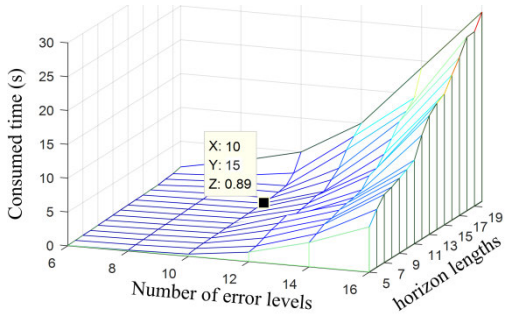

FIGURE 12. Calculation time for different combinations of error level and horizon length.

the traffic scene shown in Fig.7. The effective test road length is more than 800m. Due to the differences in driving behaviors among different drivers, it is unreasonable to compare the energy consumption of different drivers. Therefore, three GLOSA strategies listed below are adopted for each driver, and 10 groups of tests are conducted under each strategy to eliminate occasionality.

Strategy 1: free-driving without the guidance of GLOSA system; Strategy 2: GLOSA system without considering driving error; Strategy 3: GLOSA system considering driving error

B. ANALYSIS OF REAL VEHICLE EXPERIMENT

According to the hierarchical strategy, the calculation results of the upper level are updated less frequently. The global optimal results only need to be given before the departure time. However, in the real-world application, it is impossible to stop and wait for the calculation process of the upper layer, so the upper layer also needs to obtain the calculation results in a short time. Compared with the DP algorithm, PM needs less calculation time, but the computational burden is still considerable, which cannot meet the real-time application requirements of the GLOSA system. Therefore, in the real-vehicle testing, the scheme proposed in [37], which adopts the approximate model based on the speed curve instead of the upper PM, was employed to ensure that the computing time of the whole hierarchical system is within 1s.

Fig.13 shows the typical free driving trajectory without the guidance of GLOSA system. The driver tends to drive at a higher speed at first, so when it arrives at the intersection, the traffic light is still red. The vehicle needs to decelerate and stop at the intersection. When the signal turns green,

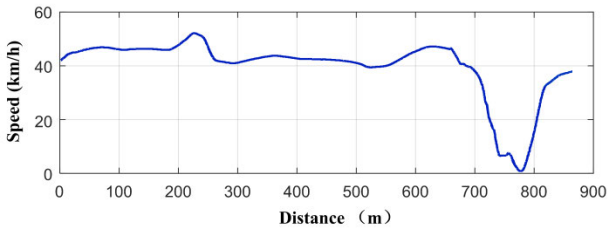

FIGURE 13. Free driving without the guidance of GLOSA system.

the vehicle accelerates to leave. Fig.14 and Fig.15 show the tracking speed and acceleration of a driver under the guidance of strategy 2 and strategy 3 in similar traffic scenes respectively.

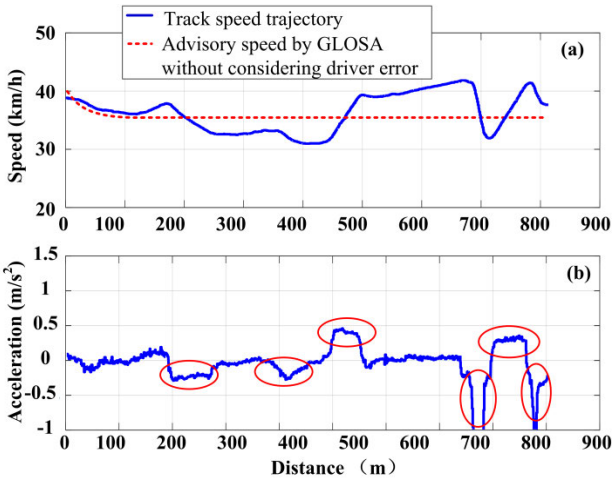

FIGURE 14. Speed and acceleration trajectories under strategy 2.

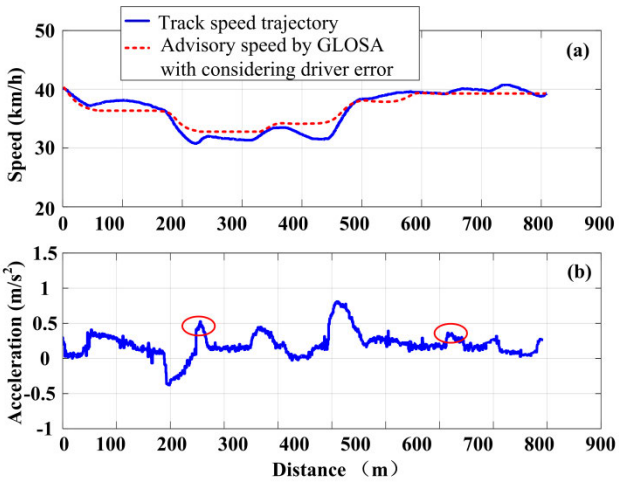

FIGURE 15. Speed and acceleration trajectories under strategy 3.

It can be seen from the tracking speed curve in Fig.14 that when considering the influence of queuing effect on the effective green light duration, the advisory speed at the beginning gradually decreases from 40km/h to 36km/h to avoid the situation where the vehicle arrives at the intersection so early that the traffic light is still red. Because the driver's driving error is not considered in the strategy 2, the recommended reference speed is not updated, resulting in the deviation between actual tracking speed and recommended speed becoming gradually larger. So that when the vehicle is approaching the intersection, the driver can only adjust the speed significantly to ensure the smooth passage of the vehicle, which is not the driving behavior we expect. It can be seen from the corresponding acceleration curve that there are many obvious abnormal acceleration and deceleration behaviors (labeled by red circles) during driving.

In Fig.15, since the GLOSA system considers the driver's tracking error, through adjusting the benchmark recommended speed, the actual tracking speed is relatively smooth, thus reducing the driver's tracking error. Although the acceleration curve also has unexpected sudden change during driving, the overall amplitude is low. Although the speed fluctuation of strategy 2 is small, the driver cannot track the constant recommended speed perfectly due to the existence of driver's tracking error. As a result, the error between the real trajectory and the optimal trajectory under Strategy 2 will increase gradually. However, despite the fact that the advisory speed of Strategy 3 fluctuates greatly, the driver's actual speed when tracking the fluctuating advisory speed is relatively smooth because the fluctuation part of the advisory speed is used to offset the driver's tracking error.

In order to show that the proposed GLOSA system can effectively affect human driving behavior, the difference between the actual speed and the reference recommended speed is calculated based on the test data of a driver in strategy 2 and strategy 3.

From Fig.16(a), the speed tracking error of the driver under strategy 2 is between −5.8km/h and 6.5km/h. 83.7% of absolute error is within 2.5km/h. The maximum error is 6.3km/h, and the average error is 1.88km/h. From Fig.16(b), the tracking speed error of the driver under strategy 3 is between −6km/h and 5.6km/h. 91.2% of absolute error is within 2.5km/h. Although the maximum absolute error is 6km/h, the average error is only 1.13km/h. Comparing the two strategies, it can be found that the speed tracking error can be reduced by 39.9% if the human driving error is considered. Because the average speed error of strategy 3 is lower than that of strategy 2, the accumulative tracking distance error of strategy 3 is much smaller.

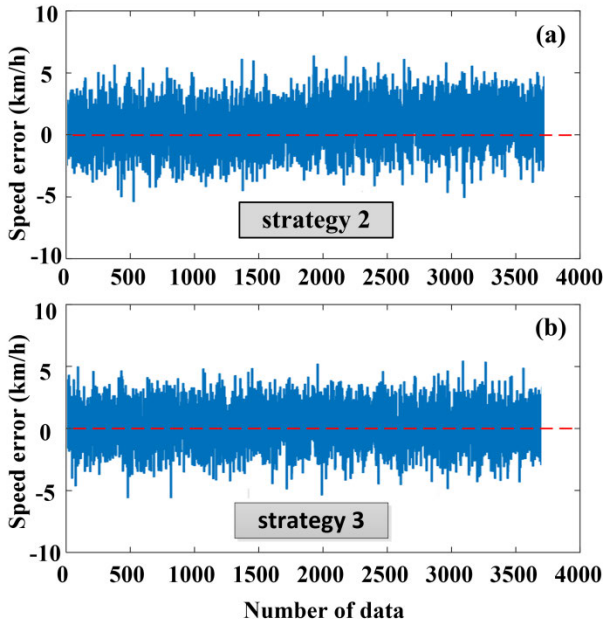

FIGURE 16. Speed tracking error under (a) strategy 2 and (b) strategy 3.

This paper further performs a hypothesis test on energy consumption to analyze the energy-saving performance of the GLOSA system. According to the collected data fragments, the speed, acceleration information and throttle signals are used to carry out the hypothesis testing combined with the motor efficiency diagram, and the average driving energy consumption of drivers under different strategies is calculated. Other energy loss factors in actual driving such as slip, slope, transmission efficiency, etc. are ignored. Table 3 shows the average energy consumption of all drivers under different strategies. It can be seen that the average driving energy consumption under strategy 3 is 4.9% lower than that of strategy 2.

TABLE 3. Average energy consumption.

Driver	strategy 2 (kWh/km)	strategy 3 (kWh/km)	3→2 savings	average
Driver 1	0.1245	0.1201	3.53%	4.9%
Driver 2	0.1233	0.1159	6.00%	
Driver 3	0.1209	0.1156	4.38%	
Driver 4	0.1167	0.1113	2.93	
Driver 5	0.1145	0.1099	4.63%	
Driver 6	0.1137	0.1047	7.92%	

Count the results of 30 road tests conducted by 6 drivers. Results showed that in 26 out of 30 experiments, drivers successfully passed the intersection after implementing the GLOSA recommended speed trajectory. There are three times encountering a small number of vehicles in front that have not fully accelerated to go through the intersection, so the main vehicle needs to slow down and switches to car-following mode. There is only one time that the vehicle needs to stop and wait. The result proves the effectiveness of our proposed method in real vehicle application.

The reasons for the above results are: (1) Because we use the average speed of traffic flow as the upper speed limit, the recommended speed is lower than other vehicles around in most cases. (2) The GLOSA system in this paper is used to guide the driver to follow the optimal advisory speed, rather than take over the control vehicle actively. Therefore, the driver can change lane to avoid collision. (3) Because for the time window constraint when planning the recommended speed, the time interval during which the front vehicles stop, accelerate and then go through the intersection has been reduced. Therefore, chances are high that the traffic flow near the intersection is smooth. Furthermore, if there is only one lane, when the vehicle in front is lower than the recommended speed of the host vehicle, the host vehicle has no choice but to switch to car-following mode. In this situation, the energy-saving performance of the vehicle will deteriorate. The optimal speed trajectory needs to be re-planned according to the new traffic situation.

VII. CONCLUSION

In this study, a hierarchical GLOSA system is designed to assist eco-driving. By estimating the queue length and calculating the effective green light duration, the optimal speed curve with minimum energy consumption is obtained in the upper layer, and the recommended reference speed is modified in the lower layer considering the human driving error, so as to reduce the speed tracking error. Compared with the GLOSA system without considering queuing effect and driving error, the proposed method can save energy consumption by 11.8% and 4.9% in simulation and real-vehicle test, respectively.

It needs to be mentioned that the application scenario of the proposed method is still very limited. The constraints are strict to some extent. The real-vehicle filed test is also insufficient due to limited experimental resources. In addition, the proposed method is effective in the case of unsaturated flow. However, for the oversaturated state, the performance of our method will degrade to some extent. More in-depth investigation needs to be conducted here. in the future, when the penetration level of connected vehicle is high, we can use the speed trajectory of connected vehicles to predict the traffic situation around and estimate the queue length. In addition, this paper only validates the proposed GLOSA system in the case of one car, more realistic scenario where there are multiple connected vehicles needs to be further researched in the future.

REFERENCES

[1] C. Zhai, F. Luo, Y. Liu, and Z. Chen, "Ecological cooperative look-ahead control for automated vehicles travelling on freeways with varying slopes," *IEEE Trans. Veh. Technol.*, vol. 68, no. 2, pp. 1208–1221, Feb. 2019.

[2] E. Ericsson, H. Larsson, and K. Brundell-Freij, "Optimizing route choice for lowest fuel consumption–potential effects of a new driver support tool," *Transp. Res. Part C, Emerg. Technol.*, vol. 14, no. 6, pp. 369–383, Dec. 2006.

[3] B. Caulfield, W. Brazil, K. N. Fitzgerald, and C. Morton, "Measuring the success of reducing emissions using an on-board eco-driving feedback tool," *Transp. Res. Part D, Transp. Environ.*, vol. 32, pp. 253–262, Oct. 2014.

[4] A. A. Malikopoulos, D. N. Assanis, and P. Y. Papalambros, "Optimal engine calibration for individual driving styles," SAE Tech. Paper 2008-01-1367, 2008, doi: 10.4271/2008-01-1367.

[5] A. A. Malikopoulos, D. N. Assanis, and P. Y. Papalambros, "Real-time self-learning optimization of diesel engine calibration," *J. Eng. Gas Turbines Power*, vol. 131, no. 2, p. 22803, Mar. 2009.

[6] J. Gonder, M. Earleywine, and W. Sparks, "Analyzing vehicle fuel saving opportunities through intelligent driver feedback," *SAE Int. J. Passenger Cars-Electron. Electr. Syst.*, vol. 5, no. 2, pp. 450–461, Apr. 2012.

[7] B. Sakhdari and N. L. Azad, "A distributed reference governor approach to ecological cooperative adaptive cruise control," *IEEE Trans. Intell. Transp. Syst.*, vol. 19, no. 5, pp. 1496–1507, May 2018.

[8] H. Suzuki and Y. Marumo, "Safety evaluation of green light optimal speed advisory (GLOSA) system in real-world signalized intersection," *J. Robot. Mechtron.*, vol. 32, no. 3, pp. 598–604, Jun. 2020.

[9] V. A. Butakov and P. Ioannou, "Personalized driver assistance for signalized intersections using V2I communication," *IEEE Trans. Intell. Transp. Syst.*, vol. 17, no. 7, pp. 1910–1919, Jul. 2016.

[10] K. Katsaros, R. Kernchen, M. Dianati, D. Rieck, and C. Zinoviou, "Application of vehicular communications for improving the efficiency of traffic in urban areas," *Wireless Commun. Mobile Comput.*, vol. 11, no. 12, pp. 1657–1667, Dec. 2011.

[11] S. Mandava, K. Boriboonsomsin, and M. Barth, "Arterial velocity planning based on traffic signal information under light traffic conditions," in *Proc. 12th Int. IEEE Conf. Intell. Transp. Syst.*, Oct. 2009, pp. 1–6.
[12] B. Asadi and A. Vahidi, "Predictive cruise control: Utilizing upcoming traffic signal information for improving fuel economy and reducing trip time," *IEEE Trans. Control Syst. Technol.*, vol. 19, no. 3, pp. 707–714, May 2011.
[13] C. Sun, X. Shen, and S. Moura, "Robust optimal ECO-driving control with uncertain traffic signal timing," in *Proc. Annu. Amer. Control Conf. (ACC)*, Jun. 2018, pp. 5548–5553.
[14] C. Zhai, Y. Liu, and F. Luo, "A switched control strategy of heterogeneous vehicle platoon for multiple objectives with state constraints," *IEEE Trans. Intell. Transp. Syst.*, vol. 20, no. 5, pp. 1883–1896, May 2019.
[15] Y. Zheng, S. E. Li, K. Li, F. Borrelli, and J. K. Hedrick, "Distributed model predictive control for heterogeneous vehicle platoons under unidirectional topologies," *IEEE Trans. Control Syst. Technol.*, vol. 25, no. 3, pp. 899–910, May 2017.
[16] X. He, H. X. Liu, and X. Liu, "Optimal vehicle speed trajectory on a signalized arterial with consideration of queue," *Transp. Res. Part C, Emerg. Technol.*, vol. 61, pp. 106–120, Dec. 2015.
[17] H. Liu, X.-Y. Lu, and S. E. Shladover, "Traffic signal control by leveraging cooperative adaptive cruise control (CACC) vehicle platooning capabilities," *Transp. Res. Part C, Emerg. Technol.*, vol. 104, pp. 390–407, Jul. 2019.
[18] S. Yu, R. Fu, Y. Guo, Q. Xin, and Z. Shi, "Consensus and optimal speed advisory model for mixed traffic at an isolated signalized intersection," *Physica A, Stat. Mech. Appl.*, vol. 531, no. 1, pp. 1–22, 2019.
[19] H. Yang, H. Rakha, and M. Venkat Ala, "Eco-cooperative adaptive cruise control at signalized intersections considering queue effects," *IEEE Trans. Intell. Transp. Syst.*, vol. 18, no. 6, pp. 1575–1585, Jun. 2017.
[20] P. Hao, G. Wu, K. Boriboonsomsin, and M. J. Barth, "Developing a framework of eco-approach and departure application for actuated signal control," in *Proc. IEEE Intell. Vehicles Symp. (IV)*, Jun./Jul. 2015, pp. 796–801.
[21] P. Hao, G. Wu, K. Boriboonsomsin, and M. J. Barth, "Preliminary evaluation of field testing on eco-approach and departure (EAD) application for actuated signals," in *Proc. Int. Conf. Connected Vehicles Expo (ICCVE)*, Oct. 2015, pp. 279–284.
[22] P. Hao, G. Wu, K. Boriboonsomsin, and M. J. Barth, "Eco-approach and departure (EAD) application for actuated signals in real-world traffic," *IEEE Trans. Intell. Transp. Syst.*, vol. 20, no. 1, pp. 30–40, Jan. 2018.
[23] P. Hao, G. Wu, K. Boriboonsomsin, and M. J. Barth, "Eco-approach and departure (EAD) application for actuated signals in real-world traffic," in *Proc. 96th Annu. Meeting Transp. Res. Board*, Washington, DC, USA, 2017, pp. 92–107.
[24] C. N. Kumar and S. C. Subramanian, "Cooperative control of regenerative braking and friction braking for a hybrid electric vehicle," *Proc. Inst. Mech. Eng., Part D, J. Automobile Eng.*, vol. 230, no. 1, pp. 103–116, Jan. 2016.
[25] M. J. Lighthill and G. B. Whitham, "On kinematic waves II. A theory of traffic flow on long crowded roads," *Proc. Roy. Soc. A, Math., Phys. Eng. Sci.*, vol. 229, no. 1178, pp. 317–345, 1955.
[26] S. Xu, K. Deng, S. E. Li, S. Li, and B. Cheng, "Legendre pseudospectral computation of optimal speed profiles for vehicle eco-driving system," in *Proc. IEEE Intell. Vehicles Symp. Proc.*, Jun. 2014, pp. 1103–1108.
[27] S. E. Li, S. Xu, X. Huang, B. Cheng, and H. Peng, "Eco-departure of connected vehicles with V2X communication at signalized intersections," *IEEE Trans. Veh. Technol.*, vol. 64, no. 12, pp. 5439–5449, Dec. 2015.
[28] S. Wei, Y. Zou, F. Sun, and O. Christopher, "A pseudospectral method for solving optimal control problem of a hybrid tracked vehicle," *Appl. Energy*, vol. 194, pp. 588–595, May 2017.
[29] J. Wu, Y. Zou, X. Zhang, G. Du, G. Du, and R. Zou, "A hierarchical energy management for hybrid electric tracked vehicle considering velocity planning with pseudospectral method," *IEEE Trans. Transport. Electrific.*, vol. 6, no. 2, pp. 703–716, Jun. 2020.
[30] S. Di Cairano, D. Bernardini, A. Bemporad, and I. V. Kolmanovsky, "Stochastic MPC with learning for driver-predictive vehicle control and its application to HEV energy management," *IEEE Trans. Control Syst. Technol.*, vol. 22, no. 3, pp. 1018–1031, May 2014.
[31] D. Moser, R. Schmied, H. Waschl, and L. del Re, "Flexible spacing adaptive cruise control using stochastic model predictive control," *IEEE Trans. Control Syst. Technol.*, vol. 26, no. 1, pp. 114–127, Jan. 2018.
[32] T. Liu, Y. Zou, D. Liu, and F. Sun, "Reinforcement learning of adaptive energy management with transition probability for a hybrid electric tracked vehicle," *IEEE Trans. Ind. Electron.*, vol. 62, no. 12, pp. 7837–7846, Dec. 2015.
[33] Y. Zou, Z. Kong, T. Liu, and D. Liu, "A real-time Markov chain driver model for tracked vehicles and its validation: Its adaptability via stochastic dynamic programming," *IEEE Trans. Veh. Technol.*, vol. 66, no. 5, pp. 3571–3582, May 2017.
[34] K. Sörensen and M. Sevaux, "A practical approach for robust and flexible vehicle routing using metaheuristics and Monte Carlo sampling," *J. Math. Model. Algorithms*, vol. 8, no. 4, pp. 387–407, Dec. 2009.
[35] S. Ferdoush and X. Li, "Wireless sensor network system design using Raspberry Pi and Arduino for environmental monitoring applications," *Procedia Comput. Sci.*, vol. 34, pp. 103–110, Jul. 2014, doi: 10.1016/j.procs.2014.07.059.
[36] A. Kesting, M. Treiber, and D. Helbing, "Enhanced intelligent driver model to access the impact of driving strategies on traffic capacity," *Phil. Trans. Roy. Soc. A, Math., Phys. Eng. Sci.*, vol. 368, no. 1928, pp. 4585–4605, Oct. 2010.
[37] X. Zhang, T. Zhang, Y. Zou, G. Du, and N. Guo, "Predictive eco-driving application considering real-world traffic flow," *IEEE Access*, vol. 8, pp. 82187–82200, 2020.

ZHAOLONG ZHANG received the M.S. degree from the Beijing Institute of Technology, China, in 2016, where he is currently pursuing the Ph.D. degree. His current research interests include vehicle dynamics control, connected cruise control, and energy-saving driving of electric vehicles.

YUAN ZOU (Senior Member, IEEE) received the Ph.D. degree from the Beijing Institute of Technology, in 2005. He is currently a Professor with the Beijing Collaborative and Innovative Center for Electric Vehicles, School of Mechanical Engineering, Beijing Institute of Technology. He is also the Co-director of the ETHZ-BIT Joint Research Center for New Energy Vehicle Dynamic System and Control. He conducted research about ground vehicle propulsion modeling and optimal control with the University of Michigan Ann Arbor and ETH Zurich. His research interests include modeling and control for electrified vehicle and transportation systems.

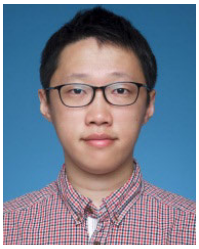

XUDONG ZHANG (Member, IEEE) received the M.S. degree in mechanical engineering from the Beijing Institute of Technology, Beijing, China, in 2011, and the Ph.D. degree in mechanical engineering from the Technical University of Berlin, Berlin, Germany, in 2017. Since 2017, he has been an Associate Professor with the Beijing Institute of Technology. His main research interests include distributed drive electric vehicles, vehicle dynamics control, vehicle state estimation, and torque allocation.

TAO ZHANG (Graduate Student Member, IEEE) received the M.S. degree from the Beijing University of Technology, China, in 2015, and the Ph.D. degree from the Beijing Institute of Technology, China, in 2020. He currently works as a Research Associate with the China North Vehicle Research Institute. His current research interests include hardware design of vehicle controller, vehicle dynamics control, advanced driver assistance systems, and reinforcement learning.